Analysis of the Overall Efficiency of a PEFC with a Bioethanol-Solar-Reforming System for Individual Houses

Shin'ya OBARA [1] and Abeer Galal El-Sayed Saad [2]

1) Power Engineering Lab., Department of Electrical and Electronic Engineering Kitami Institute of Technology

Kitami 165 Koen-cho, Kitami, Hokkaido 090-8507, Japan

E-mail: obara@mail.kitami-it.ac.jp

2) Graduate School of Engineering, Kitami Institute of Technology

Kitami 165 Koen-cho, Kitami, Hokkaido 090-8507, Japan

E-mail: brgalal@yahoo.com

Abstract

The development of a bioethanol reforming system for fuel cells (FBSR) using sunlight as a heat source was investigated. The FBSR was introduced into standard individual houses for numerical analysis. In this paper, operation of the system was analyzed by introducing two-dimensional heat diffusion equation of the catalyst layer. The supply electric power and heat were investigated using the energy-demand characteristic in a standard house in March and August in Sapporo, Japan. The overall efficiency of the production of electricity and heat power was determined by examining its thermal output characteristic. The amount of hydrogen production, the production-of-electricity characteristic, and the thermal output characteristic were examined using meteorological data in March and August. The overall efficiency of the system, defined as the rate of power and heat output compared to the amount of solar heat collected, was measured on the representative days.

Keywords: Solar Reforming, PEM Fuel Cell, Bioethanol, Heat Transfer, Simulation, Hydrogen Production, Solar Radiation

1. Introduction

The environmental impact of fuel cells changes greatly depending on the method of hydrogen production. In a detailed example, a large quantity of CO_2 is discharged when using reforming methods that employ fossil fuels. Alternatively, a fuel cell system that uses the heat of a small solar collector for the steam reforming of bioethanol, a bioethanol reforming system for fuel cells (FBSR system), has been examined [1]. Moreover, some hydrogen production technology using solar energy

is reported until now [2]. Recently, much analysis cases concerning the condensing technology of sunlight are also seen [3, 4]. There are researches on much hydrogen production technology using solar energy currently (for example, [5]). In this research, we have investigated the characteristics of the reformed gas production [1], the production-of-electricity characteristic of the FBSR using the weather forecast, and the relationship between solar insolation with fluctuation and a production-of-electricity characteristic [6]. This paper continues these reports. The main objectives of this paper are to compare the efficiency of the overall efficiency of the FBSR, and competition technology. For example, the maximum efficiency from solar energy to power of commercial silicon solar cell about 19% [7]. Moreover, we have to take into consideration power loss of a power conditioner etc., temperature characteristics of a cell, and directivity. If the overall efficiency of the proposal system is higher than competition technology, the trial production of the proposal system is effective. Moreover, in this study, fluctuation of solar radiation was taken into consideration to the reaction rate of steam reforming. There is no example of investigation of the solar reforming with solar radiation fluctuation in the past. The conversion rate of the reforming reaction of ethanol/water vapor is influenced by the temperature of a catalyst layer and the space velocity of a process gas [6]. A pellet type reforming catalyst is installed in the reactor of the FBSR. Reformed gas with a high hydrogen composition is outputted by supplying ethanol/water vapor to the reactor under the control of reactor temperature. However, because the heat source of a reactor is sunlight, the conversion rate of the fuel is affected by weather. Unsteady heat transfer analysis was introduced into the catalyst layer in a previous examination [6]. From this analysis, the transient response characteristic concerning the temperature distribution in the catalyst layer and composition of the process gas were investigated. As a result, under the weather conditions with high levels of solar radiation fluctuation over a short time, it became clear that a reforming reaction was not sufficient under the effect of a response delay. Moreover, it clarified the generation efficiency of the FBSR when taking into consideration the transient response characteristic of the reforming reaction [8]. This paper investigates the thermal output characteristic of the FBSR. The overall efficiency of the system is clarified in consideration of these results and the result of the last report. It is the objective of this paper to highlight the differences between the FBSR and competing technologies, such as commercial silicon cells. In particular, the energy flow of the system is discussed in detail.

2. System configuration

Figure 1 is a block diagram of the fuel cell system with a bioethanol solar reforming system (FBSR). The solar tracking system is introduced into two solar collectors. Moreover, each collector's collecting

area is nearly 1.0 m². Bioethanol for the boiler and the bioethanol solution for reforming are contained in a fuel tank. The S/C (molar ratio of steam to ethanol [9]) of the bioethanol solution for reforming is 3.0. Two parabolic mirrors (solar collector) with a solar tracking system are introduced into the FBSR. The heat for fuel evaporation is condensed in solar collector A while the heat for reforming of the fuel vapor is condensed in solar collector B [8].

When fuel is supplied to vaporizer, the fuel gas is fed to the reforming component. Reformed gas is supplied to the shift unit and the gas cooler, and is stored using cylinder. In order to store hydrogen, the storage tank of the reformed gas is installed in the system. While compressing and storing the reformed gas, it removes the water vapor in the gas using a cooler. Reformed gas is fed to the CO oxidation unit from the cylinder or the gas cooler, and is supplied to the fuel cell. To output power to the commercial power grid (with a regular frequency and voltage), the output of the fuel cell is converted with a DC-DC converter and an inverter. The exhaust heat from the gas cooler, the fuel cell, and the CO oxidization unit is stored. This heat is supplied to the demand side of the FBSR. When supplied solar heat is insufficient, a boiler is operated.

3. Analysis method

3.1 Basic formula

The details of the vaporizer and reactor which are installed in each Solar collector are shown in Fig. 2. As shown in Fig. 2 (a), the surface of one side of the vaporizer is heated by Solar collector A using the collected sunlight. The bioethanol solution in the vaporizer evaporates with solar heat. This steam is supplied to the reactor installed in the solar collector B (Fig. 2(b)). The reactor shown in Fig. 2 (c) is filled up with several millimeters of the spherical reforming catalyst.

Structure of the reactor and input and output of heat are shown in Fig. 3 (a). Some of solar insolation inputted from the acceptance surface on the reactor is discharged to the ambient air by convection heat transfer q_{con} and radiation heat transfer q_{rad}. Equation (1) is the heat convection of the catalyst layer, and it contains the Damkohler correction number [10]. The value of Da in Eq. (1) is calculated using Eq. (2).

$$Nu = 9.49 \cdot \left(Re \cdot Pr\right)^{0.516} \cdot \left(D_c \big/ D_{cl} \right)^{1.43} + 27.2 \cdot Da^{0.325} \tag{1}$$

$$Da = -\left(H_r \cdot \alpha_r\right) \cdot D_c \big/ \left(\rho_g \cdot u_g \cdot C_g \cdot T_g\right) \tag{2}$$

The experimental result of ethanol steam reforming using the commercial catalyst by E. Akpan et al., which is shown in Fig. 3 (b), is introduced into the analysis [11]. In this figure, the relationship between the amount of catalyst, the flow rate of ethanol, and the temperature of the catalyst layer

and the fuel conversion rate of the catalyst is depicted. The fuel conversion rate increases with an increasing amount of catalyst and with increasing temperature, as shown in Fig. 3 (b). Equation (3) is the two-dimensional heat diffusion equation of the catalyst layer. The temperature of the catalyst layer is represented by T, the coordinates of the direction of the radial direction is represented by r, and the coordinates of the direction of the catalyst layer is represented by x. A surface element is created in the direction of r, and the direction of x, about the catalyst layer of the cylinder type shown in Fig. 3 (a). Figure 3 (c) portrays the element analysis model of the catalyst layer. The element number of the catalyst layer is expressed with $el_{x,r}$ (however, $x = 1, 2, ..., N_x$, $r = 1, 2, ..., N_r$).

$$\left(\frac{\partial^2 T}{\partial r^2} + \frac{1}{r} \cdot \frac{\partial T}{\partial r} + \frac{\partial^2 T}{\partial x^2} \right) + q_{\mathrm{r}} = \frac{\rho_{\mathrm{c}} \cdot C_{\mathrm{c}}}{\lambda_{\mathrm{c}}} \cdot \frac{\partial T}{\partial t} \tag{3}$$

Boundary conditions

$$\frac{\partial T}{\partial r} = 0 \quad \text{at} \quad r = R_{cl},\ 0 \le x \le L_{cl} \tag{4}$$

$$\begin{aligned} -\lambda_{\mathrm{c}} \cdot \frac{\partial T}{\partial x} &= q_s - q_{\mathrm{rad}} - q_{\mathrm{con}} \\ &= q_s - \varepsilon \cdot \sigma \cdot \left(T_{\mathrm{s}}^4 - T_{\infty}^4 \right) - h \cdot \left(T_{\mathrm{s}} - T_{\infty} \right) \end{aligned} \tag{5}$$

$$\begin{aligned} &\text{at} \quad x = 0,\ 0 \le r \le R_{cl} \\ &\frac{\partial T}{\partial x} = 0 \quad \text{at} \quad x = L_{cl}, \quad \frac{\partial T}{\partial r} = 0 \quad \text{at} \quad r = 0 \\ &T = T_{\infty} \quad \text{for} \quad t = 0 \end{aligned} \tag{6}$$

$$\frac{\partial}{\partial x} \left(\rho_{\mathrm{g}} \cdot u_{\mathrm{g}} \right) = 0 \tag{7}$$

$$\frac{\partial u}{\partial r} = 0 \quad \text{at} \quad r = R_{cl}, \quad \frac{\partial u}{\partial x} = 0 \quad \text{at} \quad x = L_{cl} \tag{8}$$

$$u = u_0 \quad \text{at} \quad x = 0, \quad \frac{\partial u}{\partial r} = 0 \quad \text{at} \quad r = 0 \tag{9}$$

$$q_{\mathrm{r}} = g_g \cdot \psi_r \cdot H_r \tag{10}$$

3.2 Heat diffusion equation

Equation (3) is discretized, and the temperature distribution of the catalyst layer is analyzed under the boundary conditions of Eqs. (4) to (6). The central finite difference method [12] is used to

calculate the discretize Eq. (3) in this paper. Here, q_s is the heat concerning the heat exchange wall of the reactor. Equations (4) to (10) are given as the boundary condition when calculating Eq (3). Equation (6) is the boundary condition of temperature and Eq. (7) is the boundary condition of mass flow of process gas. Equations (8) and (9) are the boundary conditions of space velocity. Furthermore, Eq. (10) is the boundary condition of molar flow rate of the process gas. Equation (7) is the mass flow rate of the process gas, and Eqs. (8) and (9) are the boundary conditions in this analysis. The volume flow rate of the process gas is u_g in Eq. (7), and ρ_g is the mean density. The value u_0 in Eq. (9) is the space velocity of the fuel vapor at the entrance of the catalyst layer. This value is the result of dividing the volume flow rate of the fuel vapor by the cross section of the catalyst layer. Equation (10) expresses endothermals from the reforming reaction. Variables g_g, ψ, and H_r in Eq. (10) express the molar flow rate of process gas, the conversion ratio, and the reaction heat, respectively. If the temperature T of the catalyst layer is known, the conversion rate ψ can be obtained from the characteristic of the catalyst. Because H_r is determined by the reforming reaction, if g_g is given, the amount of endothermals q_{r} can be calculated using the reforming reaction.

4. Specification of the reforming component

The FBSR was introduced into individual houses in Sapporo, Japan. The specification of the reforming component introduced into this case analysis is described in Table 1. The heat transfer coefficient h_∞ of the convective heat transfer q_{con} was set at 10 W/m^{2}K (natural convection). Moreover, ε_{hs} of the radiation heat transfer q_{rad} gives 0.95 assuming a black body. The area A_{hs} on the heat exchange wall of the reactor is 0.005 m^2. The transmissivity of the heat exchange wall of the reactor was set at 0.9, and the condensing efficiency of the solar collector was set at 90%. In the analysis in this paper, the collecting area of solar collector A and solar collector B were both set to be 1 m^2 (unit area). In the convergence calculation of the discretization equation, an analytical accuracy of 10^{-5} was used. The use of an ethanol solution fuel supply determined that the value of the horizontal axis in Fig. 3 (b) (Amount of catalysts /Ethanol flow rate) is 35000 kg/(kmol/s).

5. Results and discussion

5.1 Temperature distribution of the catalyst layer

Figure 4 shows the analysis result of the surface temperature of the heat exchange wall. Although the influence of the outdoor air temperature to the surface temperature of the heat exchange wall is a few, the influence of the amount of solar radiation is large. Because of the wide temperature range shown in Fig. 4, the reaction velocity of the reactor changes large. Fig. 5 shows the result of the rate of filled vacancy of the amount of vapor from the vaporizer to the reactor. However, the amount of

vapor consumed by 1kW power generation of the PEFC is set as rate of filled vacancy 100%. In this paper, the rate of the heating value used for the evaporation over the amount of solar radiation by the Solar collector A is defined as efficiency of the vaporizer. The efficiency of the vaporizer of Fig. 5 is 70 to 90%. In order to maintain the rate of filled vacancy 100%, it is necessary to fulfill the conditions of the amount of insolation and outdoor air temperature.

Figure 6 shows the result of the transient response characteristic of the catalyst layer temperature when inputting constant solar insolation (250 W/m^2, 1000 W/m^2) into the reactor [6]. In Fig. 6, 0 s is the stable time of the heat exchange wall temperature after inputting solar insolation into the reactor. When the outside air temperature is 293 K, the heat exchange wall with solar irradiance of 250 W/m^2 rises to about 500 K. In the input of 1000 W/m^2, the heat exchange wall rises to about 890 K. The conversion rate of ethanol steam reforming increases, which leads to a high catalyst temperature in the reactor. Therefore, the temperature distribution of the catalyst layer shown in Fig. 6 differs so greatly that solar irradiance is large.

5.2 Composition of the process gas

Figure 7 shows the analysis result of the process gas composition of the catalyst layer when inputting constant solar insolation (250 W/m^2) into the reactor [6]. This figure shows the process gas composition along the x axis of the catalyst layer as predicted by the analysis. This figure shows the composition of each gas with its respective molar flow rate. The molar flow rate of hydrogen is larger than other gases in the composition. Distribution of the molar flow rate of hydrogen, and the time at which the hydrogen flow rate becomes stable are influenced by the magnitude of the solar irradiance input into the reactor. If there is little solar irradiance and there a short period of solar radiation fluctuation, the hydrogen generation rate may not reach the maximum possible. From this result, when there is short-time fluctuation solar radiation with little solar irradiance, the hydrogen generating rate may not reach a stable generation rate (rated speed) by a response delay.

5.3 Amount of hydrogen generation

Figure 8 shows the results of the analysis for the hydrogen generating rate as a function of sampling time. The stable time of the hydrogen generation rate is so short that much solar irradiance input to the reactor and outside air with a warm temperature. However, in realistic weather conditions, it is expected that the solar radiation fluctuates in intervals of tens of seconds. So, data from an observed amount of global solar radiation is used, and the hydrogen generating rate of FBSR are investigated under these realistic conditions. In this paper, "Surface-weather-observation 1-minute data, 2007 Sapporo district meteorological observatory,

Japan Meteorological Business Support Center" is used as observational data of the amount of global solar radiation, and outside air temperature.

Figures 9 (a) and (b) show the weather observation data (solar irradiance and outside air temperature) in 2007 August 23 and March 1 in Sapporo. In this section, proportion interpolation of the solar irradiance and the outside air temperature is considered in relation to the analysis results of Fig. 6 to Fig. 8, and the hydrogen flow rate in arbitrary weather conditions is obtained.

Figure 10 shows the analysis result of the amount of hydrogen generated by the FBSR using the amount of solar radiation, outside air temperature, and daylight hours in Sapporo in Japan. The hydrogen generating rate fluctuates a lot when comparing August 23 to March 1. From 6:00 a.m. to 11:00 a.m., the solar insolation fluctuation on the representative day in March is stable compared to that in August. The cause of this solar insolation fluctuation is a shadow by clouds. As a result, in Fig. 10, the amount of hydrogen production on a representative morning in March will be stabilized compared with that in August. As shown in Fig. 6, the rate of hydrogen generation may not be less than rated output in a weather condition with solar insolation fluctuation.

5.4 Overall efficiency

The conversion rates to the electric power are 30.7% (March representative day) and 27.1% (August representative day) every month among the solar irradiance obtained by the 1 m^2 solar collectors A and B on the representative days. On the other hand, the conversion rates to heat supply of solar irradiance are 16.7% (March representative day) and 14.8% (August representative day). Therefore, the overall efficiency of the FBSR by this operation case is 47.4% (March representative day) and 41.9% (August representative day). The difference in solar irradiance will be 1.32 times in August compared with that on the March representative day. However, the overall efficiency on the March representative day is larger than that in August. Therefore, the magnitude and the number of occurrences of the solar insolation fluctuation strongly influence the overall efficiency. Analysis results are shown in Table 2.

6. Conclusions

The overall efficiency of a PEFC with the bioethanol reforming system using a sunlight heat source (FBSR) was investigated by numerical analysis. The transient characteristic of hydrogen generation was examined based on these results. Furthermore, the supply and amount of purchase of electric power and heat were investigated using the energy-demand characteristic in a standard house in addition to meteorological data on representative days in March and August in Sapporo,

Japan. The total collecting area of the solar collectors was 2 m^2. The rate of converting sunlight into electrical power in the proposed system is 30.7% and 27.1% on representative days in March and August, respectively. On the other hand, the rate converted into heat is 16.7% and 14.8%, respectively. As a result, the overall efficiency of the FBSR by the analysis case in this paper is 47.4% and 41.9%, respectively. These results indicate that the proposed system is competitive with other energy systems, such as a photovoltaic cell. However, operation of the FBSR takes the cost of the bioethanol.

Nomenclature

C	:	Specific heat J/(g・K)
Da	:	Modified Damkohler number
el	:	The element number of the catalyst layer
g_g	:	Molar flow rate mol/s
H	:	Reaction heat J/mol
h	:	Heat transfer coefficient W/(m^2・h・K)
L	:	Length, width m
N	:	The number of elements
Nu	:	Nusselt number
P	:	Power W
Pr	:	Prandtl number
q	:	Heat W
R	:	Radius m
r	:	Radial direction of the catalyst layer
Re	:	Reynolds number
T	:	Temperature K
t	:	Sampling time s
u	:	Flow rate m/s
u_0	:	Initial flow rate m/s
x	:	Axial direction of the catalyst layer

Greek Symbols

ε	:	Emissivity
λ	:	Heat conductivity W/(m・K)
ρ	:	Density g/m^3
σ	:	Stefan-Boltzmann constant

ψ	:	Conversion ratio

Subscripts

bl	:	Boiler
c	:	Catalyst
cl	:	Catalyst layer
con	:	Convective heat transfer
cm	:	Customer
con	:	Convection
cp	:	Commercial power
dc	:	DC-DC converter
fc	:	Cell stack
g	:	Process gas
hs	:	Heat supply surface of the reactor
it	:	DC-AC converter and inverter
ox	:	The CO oxidation unit
r	:	Reforming
rad	:	Radiation
s	:	Sunlight
st	:	Storage tank
∞	:	Ambient air

Acknowledgement

This work was partially supported by a Grant-in-Aid for Scientific Research (C) from JSPS.KAKENHI (20560204).

References

[1] S. Obara and I. Tanno, Development of Distributed Energy System due to Bio-ethanol PEM Fuel Cell with Solar Reforming, Part 1—Evaluation of Basic Performance, Transactions of the Society of Heating, *Air-Conditioning and Sanitary Engineers of Japan*, 123, (2007), 23-32.

[2] C. Shen, Y. He, Y. Liu and W. Tao, Modelling and Simulation of Solar Radiation Data Processing with Simulink, Simulation Modelling Practice and Theory, Vol. 16, No. 7, 2008, 721-735.

[3] J.D. Álvarez, J.L. Guzmán, L.J. Yebra and M. Berenguel, Hybrid Modeling of Central

Receiver Solar Power Plants, Simulation Modelling Practice and Theory, Vol. 17, No. 4, 2009, 664-679.

[4] A. Steinfeld , Solar thermochemical production of hydrogen - a review, Solar Energy, Vol. 78, No. 5, 2005, 603-615.

[5] A. M. Azad, S. Kesavan, S. Al-Batty, A Closed-Loop Proposal for Hydrogen Generation Using Steel Waste and a Prototype Solar Concentrator, *International Journal of Energy Research*, Vol. 33, No. 5, 2009, 481-498.

[6] F. Fresno, R. Fernández-Saavedra, M. Belén Gómez-Mancebo, A. Vidal, M. Sánchez, M. I. Rucandio, A. J. Quejido and M. Romero, Solar Hydrogen Production by Two-Step Thermochemical Cycles: Evaluation of the Activity of Commercial Ferrites, *International Journal of Hydrogen Energy*, Vol. 34, No. 7, 2009, 2918-2924.

[7] O. Schultz, R. Preu & S.W. Glunz, Silicon Solar Cells with Screen-Printed Front Side Metallization Exceeding 19% Efficiency, *Proceedings of the 22nd European Photovoltaic Solar Energy Conference and Exhibition*, Milano, Italy, 2007, 3-7.

[8] S. Obara, Hydrogen Production Characteristics of a Bioethanol Solar Reforming System with Solar Insolation Fluctuations, *International Journal of Hydrogen Energy*, Vol. 34, No. 13, 2009, 5347-5356.

[9] J. Xuan, K.H. Leung, D. Y.C. Leung, Meng Ni, A review of biomass-derived fuel processors for fuel cell systems, *Renewable and Sustainable Energy Reviews*, Vol. 13, No. 6-7, 2009, 1301-1313.

[10] Y. Usami, S. Fukusako and M. Yamada, Heat and Mass Transfer in a Reforming Catalyst Bed (Quantitative Evaluation of the Controlling Factor by Experiment), *Transactions of the JSME*, Series B, 67(659), 2000, 1801-1808.

[11] E. Akpan, A. Akande, A. Aboudheir, H. Ibrahim and R. Idem, Experimental, Kinetic and 2-D Reactor Modeling for Simulation of the Production of Hydrogen by the Catalytic Reforming of Concentrated Crude Ethanol (CRCCE) Over a Ni-Based Commercial Catalyst in a Packed-Bed Tubular Reactor, *Chemical Engineering Science*,62(12), 2007, 3112-3126.

[12] Mitchell, Andrew Ronald, *Finite Difference and Related Methods for Differential Equations*. Wiley: New York, 2001.

Captions

Fig. 1　Block diagram

Fig. 2　PEM fuel cell system with bioethanol-solar-reforming (FBSR)

(a) Solar collector A

(b) Solar collector B

(c) Catalyst layer installed into the reactor

Fig. 3　Heat transfer analysis

(a) Input and output on the heat exchange wall of the reactor

(b) Catalyst performance)

(c) Change in the composition of process gas

Fig. 4　Temperature of the heat exchanger wall

Fig. 5　Rate of filled vacancy of the vaporizer supply

Fig. 6　Temperature distribution in the catalyst layer

(a) Outside air temperature 273K

(b) Outside air temperature 293K

(c) Outside air temperature 308K

Fig. 7　Flow rate of process gas in the catalyst layer. Outside air temperature 293 K.

(a) The amount of heat collection by the solar collector B is 250W/m^2

(b) The amount of heat collection by the solar collector B is 500W/m^2

(c) The amount of heat collection by the solar collector B is 750W/m^2

Fig. 8　Flow rate of hydrogen production

Fig. 9　Weather observation at one-minute intervals in Sapporo

(a) March 1, 2007

(b) August 23, 2007

Fig. 10　Characteristics of the hydrogen flow rate of the FBSR

(a) March 1, 2007

(b) August 23, 2007

Table 1　Analysis condition

Table 2　Analysis results of the FBSR performance

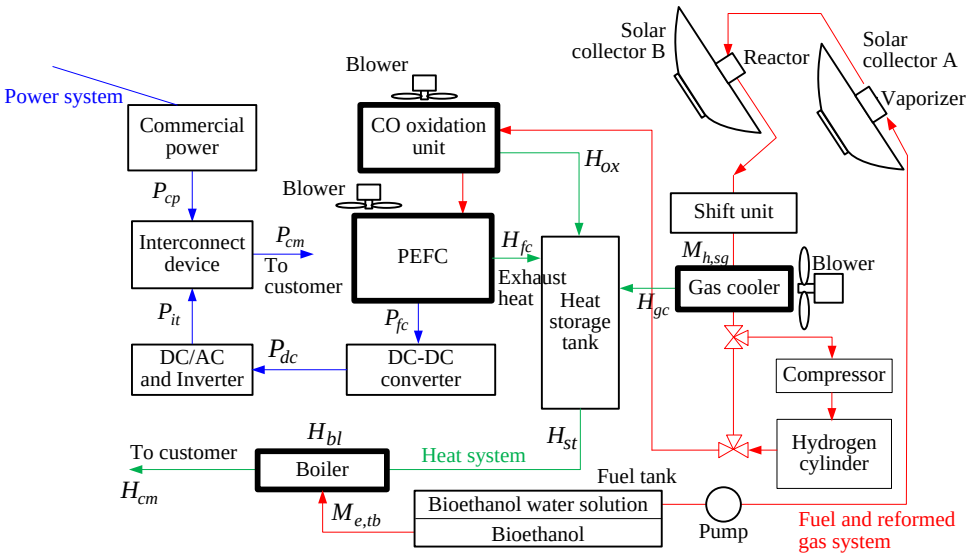

Fig. 1 Block diagram

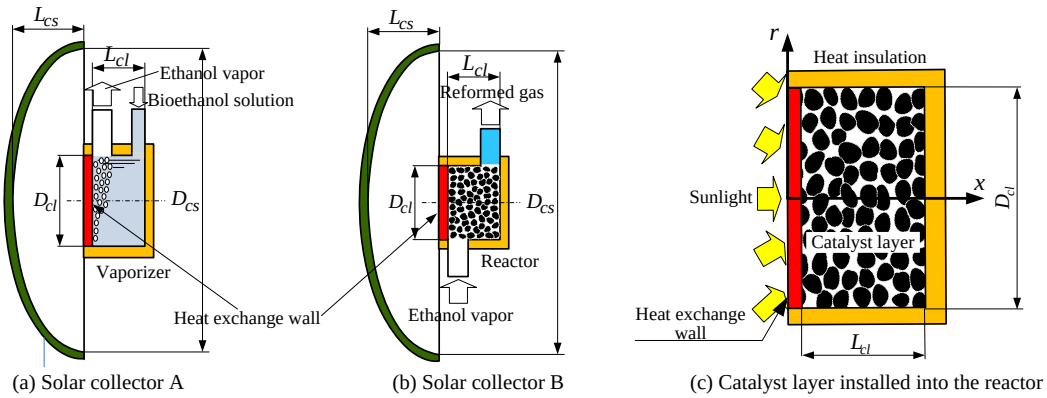

(a) Solar collector A (b) Solar collector B (c) Catalyst layer installed into the reactor

Fig. 2 PEM fuel cell system with bioethanol-solar-reforming (FBSR)

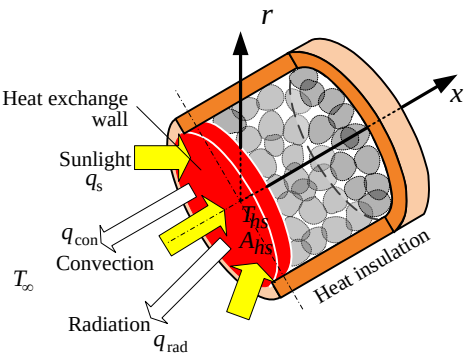

(a) Input and output on the heat exchange wall of the reactor

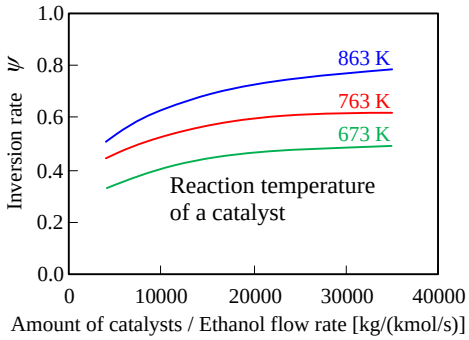

(b) Catalyst performance[)]

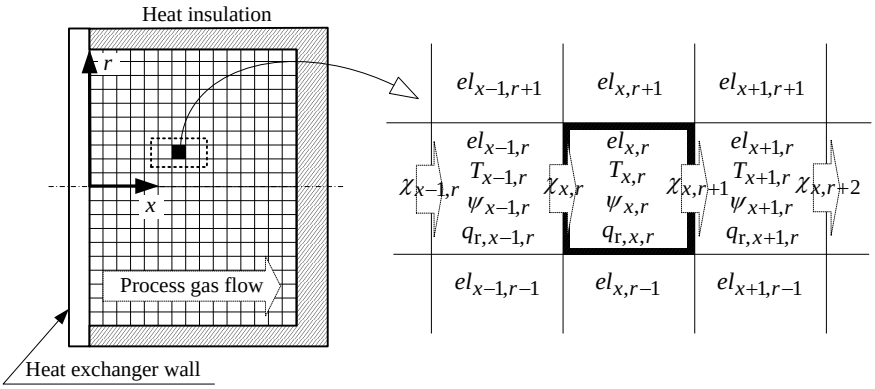

(c) Change in the composition of process gas

Fig. 3 Heat transfer analysis

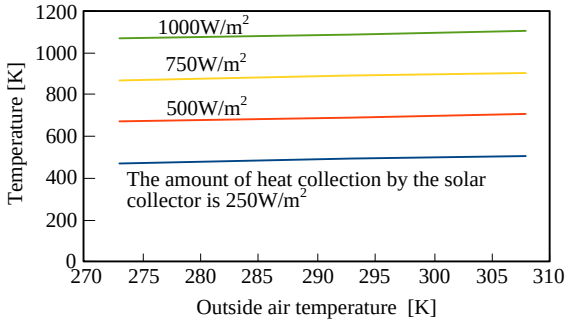

Fig. 4 Temperature of the heat exchanger wall

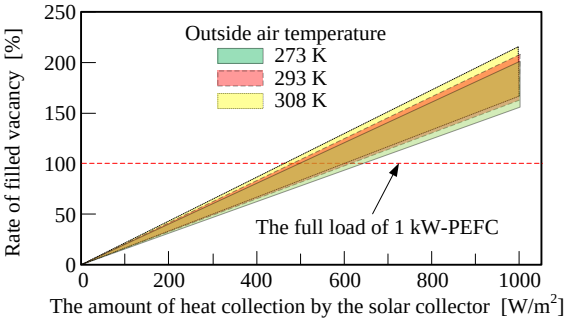

Fig. 5 Rate of filled vacancy of the vaporizer supply.
Efficiency of the vaporizer is 70-90%.

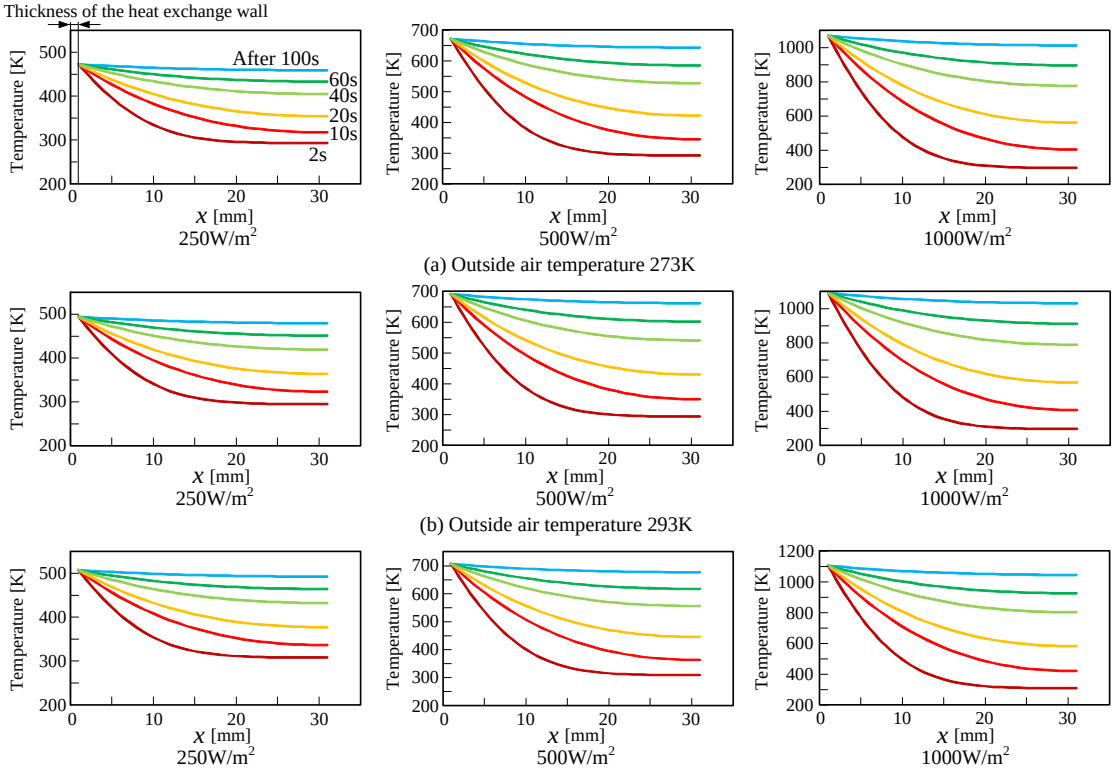

(a) Outside air temperature 273K

(b) Outside air temperature 293K

(c) Outside air temperature 308K

Fig. 6 Temperature distribution in the catalyst layer

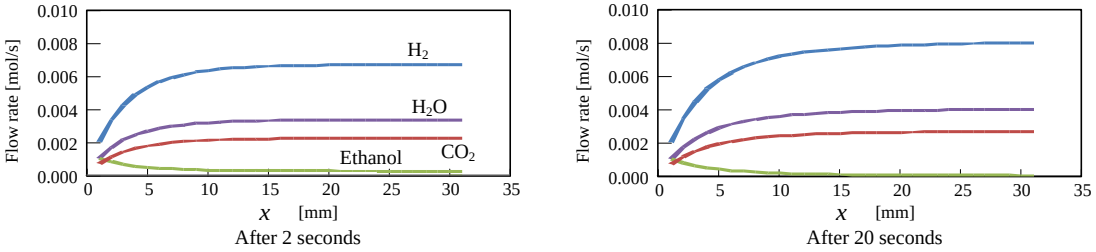

(a) The amount of heat collection by the solar collector B is 250W/m^2

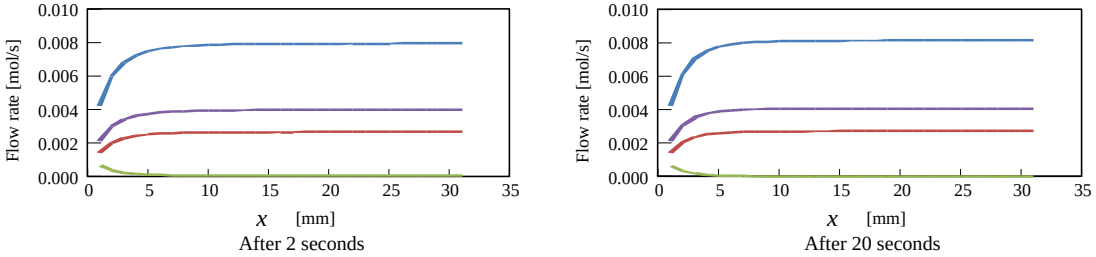

(b) The amount of heat collection by the solar collector B is 500W/m^2

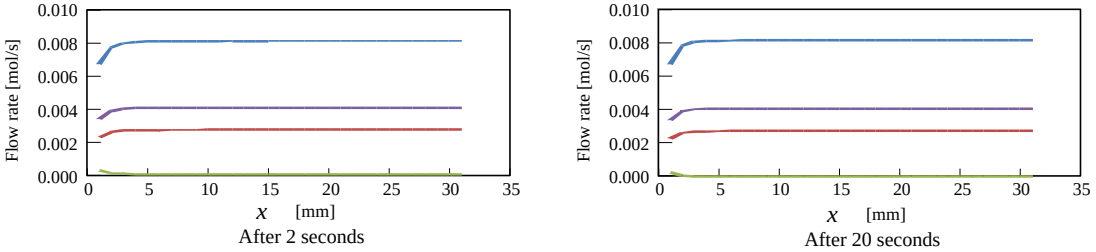

(c) The amount of heat collection by the solar collector B is 750W/m^2

Fig. 7 Flow rate of process gas in the catalyst layer. Outside air temperature 293 K.

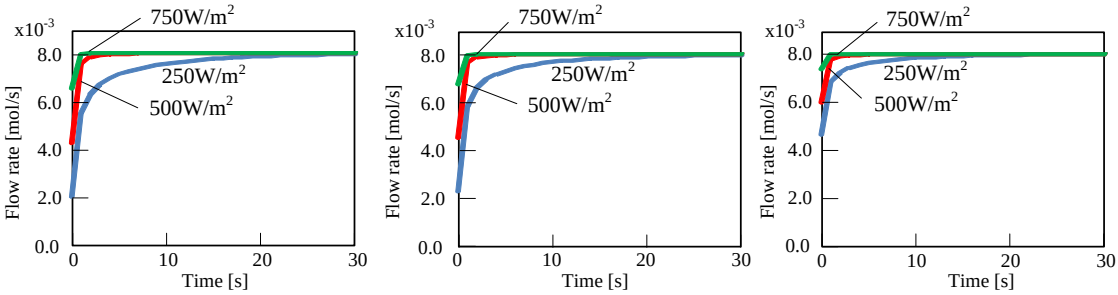

(a) 273 K (b) 293 K (c) 308 K

Outside air temperature

Fig. 8 Flow rate of hydrogen production

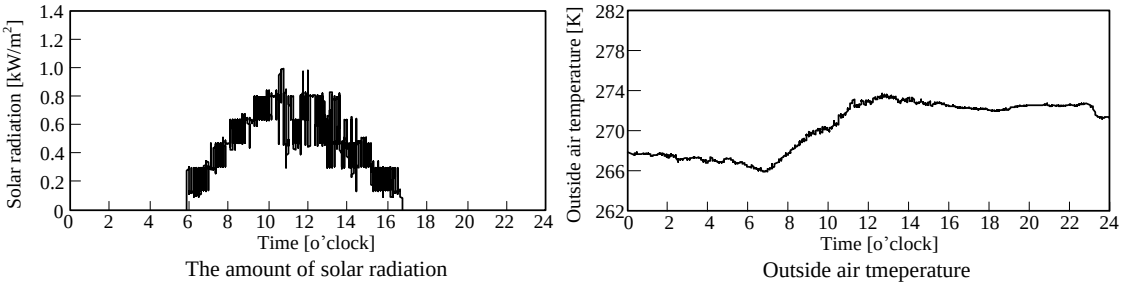

The amount of solar radiation Outside air tmeperature

(a) March 1, 2007

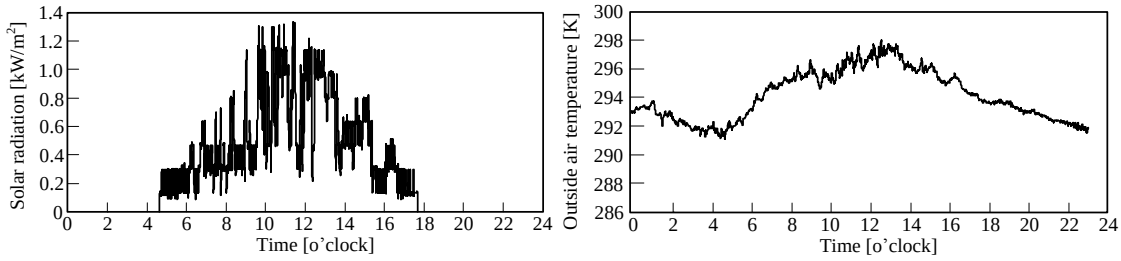

The amount of solar radiation Outside air tmeperature

(b) August 23, 2007

Fig. 9 Weather observation at one-minute intervals in Sapporo

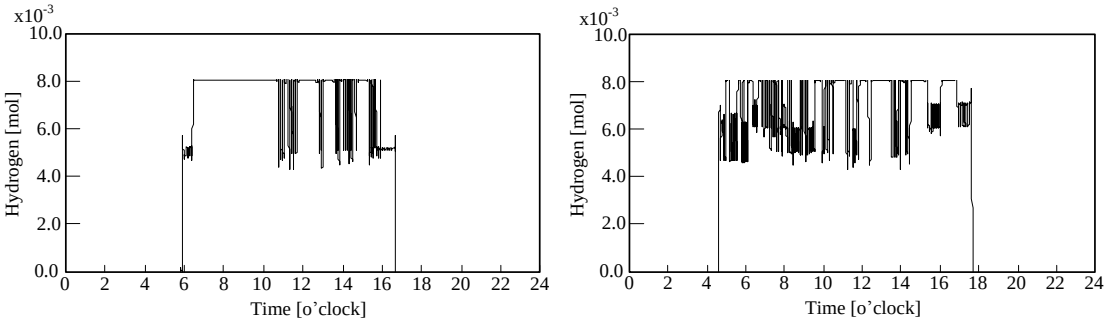

(a) March 1, 2007 (b) August 23, 2007

Fig. 10 Characteristics of the hydrogen flow rate of the FBSR

Table 1 Analysis condition

Each concentration area of the solar collector A and B	1.0 m^2
Reactor	
Length of the catalyst layer (L_{cl})	60 mm
Diameter of the catalyst layer (D_{cl})	80 mm
Particle diameter of the catalyst (D_c)	3.0 mm
Steam/carbon ratio	3.0
Catalyst filling factor	0.85
Sampling time	0.01 s
The number of element of *x*-axis (N_x)	30
The number of element of *r*-axis (N_r)	40
Density of the catalyst	213 kg/m^3
Heat conductivity of the catalyst	10 W/mK
Efficiency	
DC-DC converter (η_{dc})	95 %
DC-AC converter and inverter (η_{it})	95 %
Boiler (η_{bl})	90 %
Heat storage (η_{st})	90 %
Loss of the CO oxidation unit	3 %

Table 2 Analysis results of the FBSR performance

	March 1	August 23
Aamount of solar radiation per day by the solar collectors A and B	28.0 MJ/Day	37.0 MJ/Day
Amount of hydrogen production per day	100 g/Day	117 g/Day
Efficiency of a reforming component (The higher calorific value of hydrogen / amount of heat collections per day)	47 %	42 %
Amount of power demand per day	11.2kWh	11.0kWh
Amount of power generation per day	2.39 kWh	2.79 kWh
Amount of CO_2 emissions per day	732 g/Day	854 g/Day
Use rate of renewable energy (Condensing area 2.0 m^2)		
Power	30.7%	27.1 %
Heat	16.7 %	14.8 %
Total	**47.4 %**	**41.9 %**
System output to the quantity power demanded	21.4 %	25.3 %
System output to the quantity heat demanded (except for the boiler)	1.2 %	13.7 %